Analysis Solution Method for 3D Planar Crack Problems of Two-Dimensional Hexagonal Quasicrystals with Thermal Effects

Yuan Li[a, b], MingHao Zhao[a*], Qing-Hua Qin[b], CuiYing Fan[a]

a. School of Mechanics and Engineering Science, Zhengzhou University, Zhengzhou, Henan, 450001, China

b. Research School of Engineering, College of Engineering and Computer Science, Australian National University, Acton, ACT 2601, Australia

Abstract

An analysis solution method (ASM) is proposed for analyzing arbitrarily shaped planar cracks in two-dimensional (2D) hexagonal quasicrystal (QC) media. The extended displacement discontinuity (EDD) boundary integral equations governing three-dimensional (3D) crack problems are transferred to simplified integral-differential forms by introducing some complex quantities. The proposed ASM is based on the analogy between these EDD boundary equations for 3D planar cracks problems of 2D hexagonal QCs and those in isotropic thermoelastic materials. Mixed model crack problems under combined normal, tangential and thermal loadings are considered in 2D hexagonal QC media. By virtue of ASM, the solutions

* Corresponding author: MingHao Zhao, The School of Mechanics and Engineering Science, Zhengzhou University, No. 100 Science Road, Zhengzhou, Henan Province, 450001, P. R. of China. Tel: +86-371-67781752. E-mail: memhzhao@zzu.edu.cn, memhzhao@sina.com

to 3D planar crack problems under various types of loadings for 2D hexagonal QCs are formulated through comparison to the corresponding solutions of isotropic thermoelastic materials which have been studied intensively and extensively. As an application, analytical solutions of a penny-shaped crack subjected uniform distributed combined loadings are obtained. Especially, the analytical solutions to a penny-shaped crack subjected to the anti-symmetric uniform thermal loading are first derived for 2D hexagonal QCs. Numerical solutions obtained by EDD boundary element method provide a way to verify the validity of the presented formulation. The influences of phonon-phason coupling effect on fracture parameters of 2D hexagonal QCs are assessed.

Key words: two-dimensional hexagonal quasicrystal; three-dimensional; thermal effect; planar crack; analytical solutions; penny-shaped crack

1. Introduction

Shechtman's discovery in 1982 of a quasiperiodic crystal with sharp diffraction images of non-crystallographic symmetry [1] upset the prevailing views on the atomic structure of matter. This kind of quasiperiodic crystal was subsequently named by quasicrystal (QC) [2] which lead to the redefinition of crystals in classical crystallography, in which a solid material is either crystals or amorphous [3]. Since then, the decagonal [4], dodecagonal [5], and octagonal [6] QC phases, were synthesized and discovered in the laboratory. In 2009, a natural quasicrystal in

icosahedral phase (63%Al-24%Cu-13%Fe), was first found in a rock sample by Bindi et al. [7]. Up to 2015, the discovery of another type of natural quasicrystal with decagonal symmetry was reported [8]. Besides the above solid QCs, these quasiperiodic structures with twelve-fold and eighteen-fold symmetries were found in polymers, nanoparticle mixture and colloids, which were named soft matter QCs [9-11]. The 2011 Nobel Prize in chemistry was awarded to Shechtman owing to his exciting discovery.

QC solids with specially arranged atoms, have unique physical, chemical and mechanical properties, i.e. low surface energy, low coefficient of friction low electrical and thermal conductivity, good wear and corrosion resistance, high hardness, just to name a few [12]. Owing to these meritorious properties, several quasicrystal materials have been suggested for possible technological applications, especially in surface modified coatings and particulate-reinforcing phase for composites [13-15]. On the other hand, possible application of QC materials has been pointed out for various areas of energy savings, namely thermal insulation, light absorption, power generation and hydrogen storage [16]. Recently, the discovery of superconductivity in QCs, which is ubiquitous in many crystals, was reported by Kamiya et al [17]. In short, QCs have become a new class of functional and structural materials and have many prospective engineering applications. On account of the engineering significance and academic value, the study of QCs, has attracted considerable interest in the fields of solid-state physics, crystallography, materials science, applied mathematics, and solid mechanics [18].

Despite the bright potentials of QCs, the elasticity, defects and other subjects related to their mechanical behaviors have brought new challenge to researchers of solid mechanics [19,20]. Based on Landau density wave theory [21], two class of physical fileds, phonon and phason fields, were suggested to describe the mechanics of QCs in particular their elasticity. Since then the elastic behavior of QCs has been investigated by analysis many scholars [22-24]. According to the generalized Hooke's law to the elasticity of QCs [18,25], the fundamental equations of quasicrystals were expressed in differential form by Ding et al. [25], and the associated boundary value or initial-boundary value problems were well posed.

The analysis of QCs' crack problems, as a critical problem in solid mechanics, has attracted attention by many researchers. Due to the introduction of the extra unknown quantities and governing equations in the phason field, it is difficult to conduct crack analysis of QCs [26-28]. From the point of view of the quasiperiodic directions, QCs are classified by, respectively one-, two-, and three-dimensional QCs. 2D QCs in a 3D body have the atom arranged quasiperiodically in a plane and periodically in the orthogonal. There are ten systems, i.e. triclinic, monoclinic, orthorhombic, tetragonal, trigonal, hexagonal, pentagonal, decagonal, octagonal and dodecagonal systems, and 57 point groups in 2D QCs [29]. Mikulla et al. studied crack propagation in 2D decagonal QCs [30]. Using Fourier transform and dual integral equations theory [31], Zhou and Fan [32] calculated the displacement and stress fields, stress intensity factor and strain energy release rate for a Mode I Griffith crack in 2D octagonal QC media. Li et al. [33] investigated the asymptotic behaviour

of the stress around the Griffith crack tip in a 2D decagonal QC solid. By decomposing crack problem into a plane strain state superposed on anti-plane state problems, Guo and Fan [34] studied the Mode II crack problem of 2D decagonal QCs. Using a perturbation method, Peng and Fan considered an infinite 2D decagonal QC weakened by a circular crack and obtained the uniformly valid asymptotic solutions for the Mode I loading [35]. A meshless method, named Meshless local Petrov-Galerkin method (MLPG) was proposed by Sladek et al. [36] to investigate general crack problems in finite-size 2D decagonal quasicrystals. The references mentioned above focused on 2D plane or anti-plane crack problems only. There is less literature about 3D fracture problems of these QCs. However, crack problems should be of three-dimensional nature in practice.

Only since general solutions for 3D problems of 2D hexagonal QCs were given by Gao and Zhao [37], some research efforts have been made on the 3D crack analysis of 2D hexagonal QCs. Gao and Ricoeur [38] analytically studied the 3D problems associated with a spheroidal quasicrystalline inclusion embedded inside an infinite dissimilar quasicrystalline matrix subject to uniform loadings at infinity. As further developments to the work conducted by Gao and Zhao [37], Yang et al. [39] included thermal effect to the problem and presented the associated general solution of 2D hexagonal QCs. As an application of the general solution, they dealt with a penny-shaped crack problem with crack surface uniformly distributed temperature loadings. With the help of these general solutions in terms of quasi-harmonic functions [37,39] conjugated with the generalized method of potential theory, some

3D exact analyzes of planar crack in 2D hexagonal QCs were conducted, such as the cases of Model I crack [40] and symmetry temperature loadings [41]. Without considering thermal effects, Li et al. [42] took the phonon and phason displacement discontinuities as the unknown variables of generalized potential function method and first derived closed-form exact solutions to the elliptical crack problems for 2D hexagonal QCs. Zhao et al. [43] extended boundary integral equation method to investigate 3D planar crack problem for 2D hexagonal QCs. Due to hyper-singularity of extended displacement discontinuity (EDD) boundary integral equations derived by Zhao et al. [43], it is difficult to solve these integral equations analytically via the conventional methods. An EDD boundary element formulation was proposed by Li et al. [44] to study 3D planar crack problems of 2D hexagonal QCs with thermal effects. By virtue of EDD boundary element method, Li et al. [44] presented numerical results for rectangular, elliptical and penny-shaped crack.

Although, numerical method [36, 44, 45] is very convenient to solve all kinds of planar crack problems, corresponding analytical solutions are more advantageous in revealing coupling relationships between various physic fields and are of more theoretical and practical significance. The present paper explores an analysis solution method (ASM) to investigate 3D planar cracks of 2D hexagonal QCs. Some analytical solutions to 3D crack problems of these QCs are given for the first time. Following this introduction., the 3D planar crack problem considered is stated in Section 2. The EDD boundary integral equations derived by Zhao et al. [43] are presented in Section 3, which are the basic equations to build our analytical approach of ASM. Section 4

presents the solution procedure of ASM for various kinds of crack modes. As an application of the ASM, the analytical solutions of a penny-shape crack with uniformly combined loadings applied on crack surfaces are presented in Section 5. In Section 6, the solution derived from the proposed ASM is verified by EDD boundary element method [44] and numerically presented to discuss the influences of phonon-phason couple effects on fracture parameters of 2D hexagonal QCs. Finally, some conclusions drawn from the present study are given in Section 7.

2. Statement of the problems

We describe a 2D QC medium, possessing the point groups of *6mm*, 622, $\overline{6}m2$, *6/mmm* and Laue class 10 [18], in a Cartesian coordinate system (*x*, *y*, *z*) with the quasiperiodic plane of QCs parallel to the plane *oxy*. An arbitrarily shaped planar crack S lies on the plane *oxy*, as shown in Figure 1. The upper and lower surfaces of the crack S are denoted by S^+ and S^-, respectively. The outer normal vectors of S+ and S− have the relation

$$\{n_i\}_{S^+} = \{0, 0, -1\}, \quad \{n_i\}_{S^-} = \{0, 0, 1\}. \tag{1}$$

It is assumed that the arbitrarily extended tractions, namely combined loadings, are applied on crack surfaces. The extended tractions including not only conventional phonon tractions p_i, but also phason tractions q_i, and heat flux boundary value h_n, have the same magnitude but opposite directions on the upper and lower crack surfaces, i.e.,

$$p_i \mid_{s^+} = -p_i \mid_{s^-}, \quad q_i \mid_{s^+} = -q_i \mid_{s^-}, \quad h_n \mid_{s^+} = -h_n \mid_{s^-}, \tag{2}$$

where

$$\begin{aligned} p_i &= \sigma_{ij} n_j, \\ q_i &= H_{ij} n_j, \quad (i, j = 1, 2, 3 \text{ or } x, y, z,), \\ h_n &= h_i n_i, \end{aligned} \tag{3}$$

$\sigma_{ij} \left(H_{ij} \right)$ and h_i are the components of phonon (phason) stress and heat flux, respectively. According to Landau density wave theory, besides the conventional phonon fields, phason fields are introduced to determine the local rearrangement of atoms in a cell in QCs [19,25]. Identical to the standard elasticity of crystals, the phonon stress tensor is symmetric, i.e., $\sigma_{ij} = \sigma_{ji}$, however, the phason stress tensor is asymmetry, as $H_{ij} \neq H_{ji}$. For 2D QCs, the phonon stress has explicit components $\{ \sigma_{xx}, \sigma_{yy}, \sigma_{zz}, \sigma_{xy}, \sigma_{yz}, \sigma_{zx} \}$ and phason stress $\{ H_{xx}, H_{yy}, H_{xy}, H_{yx}, H_{yz}, H_{xz} \}$ [19,37].

The existence of the crack causes the phonon (phason) displacements $u(w)$, displacements and temperature change θ across the crack surfaces to be discontinuous. We define that

$$\| u_i \| = u_i \mid_{S^+} - u_i \mid_{S^-}, (i = 1, 2, 3, \text{ or } x, y, z), \tag{4a}$$

$$\| w_j \| = w_j \mid_{S^+} - w_j \mid_{S^-}, \quad (j = 1, 2, \text{ or } x, y), \tag{4b}$$

$$\| \theta \| = \theta \mid_{S^+} - \theta \mid_{S^-}, \tag{4c}$$

These are referred to as the extended displacement discontinuities (EDDs) to characterize fracture properties of 2D hexagonal QCs. Additionally, the basic equations including the constitutive equations and the equilibrium equations for are specified in Appendix A.

3. EDD boundary integral equations for 3D arbitrarily shaped planar crack problems

Using Green's functions of unit point EDDs and the superposition principal [45], Zhao et al. [43] obtained the EDD boundary integral equations for 3D arbitrarily shaped planar crack problems in 2D hexagonal QC media, i.e.,

$$\int_{S^+}\left\{\frac{1}{r^3}\left[\left(3\cos^2\phi-1\right)\left(L_{11}\|u_x\|+L_{w11}\|w_x\|\right)+\left(3\sin^2\phi-1\right)\left(L_{12}\|u_x\|+L_{w12}\|w_x\|\right)\right]\right.$$
$$\left.+\left(L_{13}\|u_y\|+L_{w13}\|w_y\|\right)\cos\phi\sin\phi\frac{1}{r^3}+L_{1\theta}\cos\phi\frac{1}{r^2}\|\theta\|\right\}dS(\xi,\eta)=-p_x(x,y), \tag{5a}$$

$$\int_{S^+}\left\{\frac{1}{r^3}\left[\left(3\cos^2\phi-1\right)\left(L_{11}\|u_y\|+L_{w11}\|w_y\|\right)+\left(3\sin^2\phi-1\right)\left(L_{12}\|u_y\|+L_{w12}\|w_y\|\right)\right]\right.$$
$$\left.+\left(L_{13}\|u_x\|+L_{w13}\|w_x\|\right)\cos\phi\sin\phi\frac{1}{r^3}+L_{1\theta}\cos\phi\frac{1}{r^2}\|\theta\|\right\}dS(\xi,\eta)=-p_y(x,y), \tag{5b}$$

$$\int_{S^+}\left\{\frac{1}{r^3}\left[\left(3\cos^2\phi-1\right)\left(L_{21}\|u_x\|+L_{w21}\|w_x\|\right)+\left(3\sin^2\phi-1\right)\left(L_{22}\|u_x\|+L_{w22}\|w_x\|\right)\right]\right.$$
$$\left.+\left(L_{23}\|u_y\|+L_{w23}\|w_y\|\right)\cos\phi\sin\phi\frac{1}{r^3}+L_{2\theta}\cos\phi\frac{1}{r^2}\|\theta\|\right\}dS(\xi,\eta)=-q_x(x,y), \tag{5c}$$

$$\int_{S^+}\left\{\frac{1}{r^3}\left[\left(3\cos^2\phi-1\right)\left(L_{21}\|u_y\|+L_{w21}\|w_y\|\right)+\left(3\sin^2\phi-1\right)\left(L_{22}\|u_y\|+L_{w22}\|w_y\|\right)\right]\right.$$
$$\left.+\left(L_{23}\|u_x\|+L_{w23}\|w_x\|\right)\cos\phi\sin\phi\frac{1}{r^3}+L_{2\theta}\cos\phi\frac{1}{r^2}\|\theta\|\right\}dS(\xi,\eta)=-q_y(x,y), \tag{5d}$$

$$\int_{S^+}L_3\frac{\|u_z\|}{r^3}dS(\xi,\eta)=-p_z(x,y), \tag{5e}$$

$$\int_{S^+}L_h\frac{\|\theta\|}{r^3}dS(\xi,\eta)=-h_n(x,y), \tag{5f}$$

where

$$r=\sqrt{(\xi-x)^2+(\eta-y)^2}, \tag{6a}$$

$$\cos\phi=\frac{(\xi-x)}{r}, \qquad \sin\phi=\frac{(\eta-y)}{r}, \tag{6b}$$

and L_{ij}, L_{wij}, L_3 and L_h are the material-related constants which are listed in

Appendix B, or can be found in Ref [43].

EDD boundary integral equations (5a-f) are the governing equations of crack boundary value problems stated in Section 2. In Eq. (5), the problem can be decoupled into three cases: **1)** crack problem under normal loading which is governed by Eq (5e); **2)** crack problem under the phonon (phason) tangential loadings governed by Eqs(5a-d); **3)** crack problem under the thermal loadings governed by Eqs. (5a-d) and (5f) [43]. The complexity of Eq. (5) makes it difficult to obtain analytical solution via conventional methods, especially for Eq. (5a-d) governing the tangential problem. The numerical method based on EDD boundary element method proposed by Li et al. [44] can be used to solve Eq. (5).

When the EDDs are determined by solving Eq. (5), the extended stress intensity factors can be obtained in term of the following relationships [43].

$$K_{\mathrm{I}}^{\mathrm{F}} = \sqrt{2\pi}\pi \lim_{\rho \to 0} L_3 \left\| u_z \right\| / \sqrt{\rho}, \qquad (7a)$$

$$K_{\mathrm{II}}^{\mathrm{F}} = \sqrt{2\pi}\pi \lim_{\rho \to 0} \left(L_{11} \left\| u_x \right\| + L_{w11} \left\| w_x \right\| \right) / \sqrt{\rho},$$

$$K_{\mathrm{III}}^{\mathrm{F}} = \sqrt{2\pi}\pi \lim_{\rho \to 0} \left(L_{12} \left\| u_y \right\| + L_{w12} \left\| w_y \right\| \right) / \sqrt{\rho}, \qquad (7b)$$

$$K_{\mathrm{II}}^{\mathrm{H}} = \sqrt{2\pi}\pi \lim_{\rho \to 0} \left(L_{21} \left\| u_x \right\| + L_{w21} \left\| w_x \right\| \right) / \sqrt{\rho},$$

$$K_{\mathrm{III}}^{\mathrm{H}} = \sqrt{2\pi}\pi \lim_{\rho \to 0} \left(L_{22} \left\| u_y \right\| + L_{w22} \left\| w_y \right\| \right) / \sqrt{\rho}, \qquad (7c)$$

$$K_{\mathrm{h}} = \sqrt{2\pi}\pi \lim_{\rho \to 0} L_{\mathrm{h}} \left\| \theta \right\| / \sqrt{\rho}, \qquad (7d)$$

where $K_{\mathrm{I}}^{\mathrm{F}}$ is Mode I phonon stress intensity factor, $K_{\mathrm{II}}^{\mathrm{F}}\left(K_{\mathrm{II}}^{\mathrm{H}}\right)$ is Mode II phonon (phason) stress intensity factor, $K_{\mathrm{III}}^{\mathrm{F}}\left(K_{\mathrm{III}}^{\mathrm{H}}\right)$ is Mode III stress intensity factor, K_{h} is heat flux intensity factor, and ρ is the distance of a point on crack face to the crack border.

4. Solution procedure of ASM for an arbitrarily shaped planar crack

4.1. Crack surfaces subjected to normal loading

The problem with crack surfaces subjected to normal loading ($p_z(x, y)$) is governed by Eq. (5e). Consider the same problem but for isotropic elastic materials, the corresponding displacement discontinuity boundary integral equation takes the form [47,48]

$$\frac{E}{8\pi(1-v^2)}\int_{S^+}\frac{\|u_z^e\|}{r^3}\mathrm{d}S = -p_z(x,\, y),\qquad(8)$$

where E and v are Young's modulus and Poisson's ratio, respectively, and superscript "e" represents corresponding quantity in the isotropic elasticity. In addition, the Mode I stress intensity factor can be obtained through [47]

$$K_{\mathrm{I}}^e = \frac{E}{8(1-v^2)}\lim_{\rho\to0}\sqrt{\frac{2\pi}{\rho}}\|u_z^e\|.\qquad(9)$$

Comparing Eq. (5e) to Eq. (8), we can see that for 2D hexagonal QCs, the unknown quantity $\|u_z\|$ in Eq. (5f) can be solved by

$$\|u_z\| = \frac{1}{L_3}\frac{E}{8\pi(1-v^2)}\|u_z^e\|.\qquad(10)$$

Substituting Eq. (10) to Eq. (7a), the Mode I stress intensity factor for 2D hexagonal QCs is obtained as

$$K_{\mathrm{I}}^{\mathrm{F}} = K_{\mathrm{I}}^e.\qquad(11)$$

It should be noted that the crack solutions of EDD, or $K_{\mathrm{I}}^{\mathrm{F}}$ for 3D planar crack problems in 2D hexagonal QCs media can be calculated by Eqs. (10) and (11) with

the corresponding solutions of isotropic elastic materials.

4.2. Crack surfaces subjected to tangential loadings

From Eq.(5), we find that the temperature discontinuity $\|\theta\|$ exists in Eqs. (5a-d) and (5f), but it only depends on heat flux crack boundary value in Eq.(5f). If there is no thermal loading, $\|\theta\|$ becomes zero. Therefore, the crack problem under the phonon (phason) tangential loadings is only governed by Eqs. (5a-d). It is easily seen that Eqs. (5a-d) are coupled with each other which makes the solution finding more complicated. In order to simplify Eqs. (5a-d), we introduce the following complex quantities:

$$U = u_x + iu_y, \ W = w_x + iw_y,$$
$$P = p_x + ip_y, \ Q = q_x + iq_y, \tag{12}$$

where $i = \sqrt{-1}$, with this introduction, equations (5a-d) are simplified and transferred to the following concise form

$$\int_{S^+}\left\{\Delta\frac{1}{r}\begin{bmatrix}L_1 & L_{w1}\\ L_2 & L_{w2}\end{bmatrix}\begin{bmatrix}\|U\|\\ \|W\|\end{bmatrix}+\Lambda^2\frac{1}{r}\begin{bmatrix}\overline{L}_1 & \overline{L}_{w1}\\ \overline{L}_2 & \overline{L}_{w2}\end{bmatrix}\begin{bmatrix}\|\overline{U}\|\\ \|\overline{W}\|\end{bmatrix}\right\}dS = -\begin{bmatrix}P(x,\ y)\\ Q(x,\ y)\end{bmatrix}, \tag{13}$$

where $\Delta = \partial^2/\partial x^2 + \partial^2/\partial y^2$, $\Lambda = \partial/\partial x + i\partial/\partial y$, and

$$L_1 = \frac{L_{11}+L_{12}}{2}, \ L_{w1} = \frac{L_{w11}+L_{w12}}{2},$$
$$\overline{L}_1 = \frac{L_{11}-L_{12}}{2}, \ \overline{L}_{w1} = \frac{L_{w11}-L_{w12}}{2}, \tag{14a}$$

$$L_2 = \frac{L_{21}+L_{22}}{2}, \ L_{w2} = \frac{L_{w21}+L_{w22}}{2},$$
$$\overline{L}_2 = \frac{L_{21}-L_{22}}{2} \ \overline{L}_{w2} = \frac{L_{w21}-L_{w22}}{2}. \tag{14b}$$

By denoting

$$K^{\mathrm{F}} = K_{\mathrm{II}}^{\mathrm{F}} + iK_{\mathrm{II}}^{\mathrm{F}},$$
$$K^{\mathrm{H}} = K_{\mathrm{II}}^{\mathrm{H}} + iK_{\mathrm{II}}^{\mathrm{H}}, \tag{15}$$

equations (7b) and (7c) become

$$\begin{bmatrix} K^{\mathrm{F}} \\ K^{\mathrm{H}} \end{bmatrix} = \sqrt{2\pi}\,\pi \lim_{\rho \to 0} \left(\begin{bmatrix} L_1 & L_{w1} \\ L_2 & L_{w2} \end{bmatrix} \begin{bmatrix} \|U\| \\ \|W\| \end{bmatrix} + \begin{bmatrix} \overline{L}_1 & \overline{L}_{w1} \\ \overline{L}_2 & \overline{L}_{w2} \end{bmatrix} \begin{bmatrix} \|\overline{U}\| \\ \|\overline{W}\| \end{bmatrix} \right) \frac{1}{\sqrt{\rho}}. \tag{16}$$

For isotropic elastic media, we have [47]

$$\int_{S^+} \left[\Delta \frac{1}{r} \frac{E(2-v)}{16\pi(1-v^2)} \|U^e\| + \Lambda^2 \frac{1}{r} \frac{Ev}{16\pi(1-v^2)} \|\overline{U}^e\| \right] \mathrm{d}S = -T(x,y), \tag{17}$$

where $T(x,y)$ is the tangential loading, and

$$K^e = K^e_{\mathrm{II}} + \mathrm{i}K^e_{\mathrm{III}} = \sqrt{2\pi}\,\pi \lim_{\rho \to 0} \left[\frac{E(2-v)}{16\pi(1-v^2)} \|U\| + \frac{Ev}{16\pi(1-v^2)} \|\overline{U}\| \right] \Big/ \sqrt{\rho}. \tag{18}$$

We suppose there are two different isotropic elastic media with corresponding quantities E_1, v_1, T_1 and E_2, v_2, T_2, and the tangential loadings T_1 and T_2 have the same magnitude with phonon and phason loadings, i.e., $T_1(x,y) = P(x,y)$, and $T_2(x,y) = Q(x,y)$. According to Eqs. (17) and (18), one has

$$\int_{S^+} \left\{ \Delta \frac{1}{r} \begin{bmatrix} \dfrac{E_1(2-v_1)}{16\pi(1-v_1^2)} \|U_1^e\| \\ \dfrac{E_2(2-v_2)}{16\pi(1-v_2^2)} \|U_2^e\| \end{bmatrix} + \Lambda^2 \frac{1}{r} \begin{bmatrix} \dfrac{E_1 v_1}{16\pi(1-v_1^2)} \|\overline{U}_1^e\| \\ \dfrac{E_2 v_2}{16\pi(1-v_2^2)} \|\overline{U}_2^e\| \end{bmatrix} \right\} \mathrm{d}S = - \begin{bmatrix} P(x,y) \\ Q(x,y) \end{bmatrix}, \tag{19}$$

and

$$\begin{bmatrix} K_1^e \\ K_2^e \end{bmatrix} = \sqrt{2\pi}\,\pi \lim_{\rho \to 0} \left(\begin{bmatrix} \dfrac{E_1(2-v_1)}{16\pi(1-v_1^2)} \|U_1^e\| \\ \dfrac{E_2(2-v_2)}{16\pi(1-v_2^2)} \|U_2^e\| \end{bmatrix} + \begin{bmatrix} \dfrac{E_1 v_1}{16\pi(1-v_1^2)} \|\overline{U}_2^e\| \\ \dfrac{E_2 v_2}{16\pi(1-v_2^2)} \|\overline{U}_2^e\| \end{bmatrix} \right) \frac{1}{\sqrt{\rho}}. \tag{20}$$

On letting

$$\begin{bmatrix} L_1 & L_{w1} \\ L_2 & L_{w2} \end{bmatrix} \begin{bmatrix} \|U\| \\ \|W\| \end{bmatrix} = \begin{bmatrix} \dfrac{E_1(2-v_1)}{16\pi(1-v_1^2)} \|U_1^e\| \\ \dfrac{E_2(2-v_2)}{16\pi(1-v_2^2)} \|U_2^e\| \end{bmatrix}, \tag{21a}$$

$$\begin{bmatrix} \overline{L}_1 & \overline{L}_{w1} \\ \overline{L}_2 & \overline{L}_{w2} \end{bmatrix} \begin{bmatrix} \|\overline{U}\| \\ \|\overline{W}\| \end{bmatrix} = \begin{bmatrix} \dfrac{E_1 \nu_1}{16\pi(1-\nu_1^2)}\|\overline{U}_1^e\| \\ \dfrac{E_2 \nu_2}{16\pi(1-\nu_2^2)}\|\overline{U}_2^e\| \end{bmatrix}, \tag{21b}$$

it is found that Eqs. (13) and (19) are identical in terms of structure. Thus, $\|U\|$ and $\|W\|$ can be directly obtained from the corresponding elastic solutions from Eq.(21a), or Eq.(21b) as follows

$$\begin{bmatrix} \|U\| \\ \|W\| \end{bmatrix} = \begin{bmatrix} L_1 & L_{w1} \\ L_2 & L_{w2} \end{bmatrix}^{-1} \begin{bmatrix} \dfrac{E_1(2-\nu_1)}{16\pi(1-\nu_1^2)}\|U_1^e\| \\ \dfrac{E_2(2-\nu_2)}{16\pi(1-\nu_2^2)}\|U_2^e\| \end{bmatrix}, \tag{22a}$$

$$\begin{bmatrix} \|\overline{U}\| \\ \|\overline{W}\| \end{bmatrix} = \begin{bmatrix} \overline{L}_1 & \overline{L}_{w1} \\ \overline{L}_2 & \overline{L}_{w2} \end{bmatrix}^{-1} \begin{bmatrix} \dfrac{E_1 \nu_1}{16\pi(1-\nu_1^2)}\|\overline{U}_1^e\| \\ \dfrac{E_2 \nu_2}{16\pi(1-\nu_2^2)}\|\overline{U}_2^e\| \end{bmatrix}. \tag{22b}$$

To make Eqs. (22a) and (22b) identical with each other, ν_1 and ν_2 should satisfy the following relationship

$$\frac{2-\nu_1}{\nu_1} = \frac{L_1\|U\| + L_{w1}\|W\|}{\overline{L}_1\|U\| + \overline{L}_{w1}\|W\|}, \tag{23a}$$

$$\frac{2-\nu_2}{\nu_2} = \frac{L_2\|U\| + L_{w2}\|W\|}{\overline{L}_2\|U\| + \overline{L}_{w2}\|W\|}. \tag{23b}$$

Observing Eqs. (19), (21) and (23), one can find that if $\|U\|/\|W\|$ is constant, ν_1 and ν_2 can be solved by Eq.(23).

Substituting Eq. (21) into Eq. (16) and comparing it with Eq. (20), we can obtain

$$\begin{bmatrix} K^{\mathrm{F}} \\ K^{\mathrm{H}} \end{bmatrix} = \begin{bmatrix} K_1^e \\ K_2^e \end{bmatrix}. \tag{24}$$

Note that from Eq. (24), it looks like that the phonon and phason stress intensity factors ($K^{\mathrm{F}}, K^{\mathrm{H}}$) are decoupled and depend on the phonon and phason loadings,

respectively, however, from Eq. (20), expressions of both K_1^e and K_2^e include v_1 and v_2, respectively. Since v_1 and v_2 are coupled with each other as indicated in Eq. (18) and must depend on both phonon and phason loadings, and K^{F} and K^{H} are actually coupled. With v_1 and v_2 being determined by Eq. (23), K^{F} and K^{H} can be calculated by Eq. (24) directly using the corresponding solutions of purely elastic material which has been studied intensively and extensively.

4.3. Crack surfaces subjected to thermal loading

We assume that only thermal loading is applied on the crack surfaces. This problem is governed by Eq.(5a-d) and (5f). However, the temperature discontinuity $\|\theta\|$ depends on Eq. (5f) only. For the same problem for isotropic thermoelastic material, there is a similar governing boundary equation [47,48] as

$$\frac{\beta}{4\pi} \int_{S^+} \frac{\|\theta^e\|}{r^3} \mathrm{d}S = h_n(x, y), \tag{25}$$

and the heat flux intensity factor is

$$K_{\mathrm{h}}^e = -\frac{\beta}{4} \sqrt{2\pi} \lim_{\rho \to 0} \frac{\|\theta\|}{\sqrt{\rho}}, \tag{26}$$

where β is the coefficient of heat conduction. Comparing Eq. (5f) to Eq. (25), the temperature discontinuity $\|\theta\|$ for 2D hexagonal QCs can be solved by

$$\|\theta\| = -\frac{\beta}{4\pi L_{\mathrm{h}}} \|\theta^e\|, \tag{27}$$

and the heat flux intensity factor is

$$K^{\mathrm{h}} = K_e^{\mathrm{h}}. \tag{28}$$

Substituting Eq. (27) into Eqs. (5a-d) with Eq. (13) yields

$$\int_{S^+}\left\{\Delta\frac{1}{r}\begin{bmatrix}L_1 & L_{w1}\\ L_2 & L_{w2}\end{bmatrix}\begin{bmatrix}\|U\|\\ \|W\|\end{bmatrix}+\Lambda^2\frac{1}{r}\begin{bmatrix}\overline{L}_1 & \overline{L}_{w1}\\ \overline{L}_2 & \overline{L}_{w2}\end{bmatrix}\begin{bmatrix}\|\overline{U}\|\\ \|\overline{W}\|\end{bmatrix}\right\}dS=\frac{\beta}{4\pi L_h}\begin{bmatrix}L_{1\theta}\\ L_{2\theta}\end{bmatrix}\int_{S^+}\Lambda\frac{1}{r}\|\theta^e\|dS,\quad(29)$$

which can be regarded as a tangential problem just like the subsection above. Therefore, two systems of isotropic material are used. The displacement discontinuity boundary integral equations for isotropic thermoelastic problem [48] are transferred to

$$\int_{S^+}\left\{\Delta\frac{1}{r}\begin{bmatrix}\frac{2-\nu_1}{2}\|U_1^\theta\|\\[4pt]\frac{2-\nu_2}{2}\|U_2^\theta\|\end{bmatrix}+\Lambda^2\frac{1}{r}\begin{bmatrix}\frac{\nu_1}{2}\|\overline{U}_1^\theta\|\\[4pt]\frac{\nu_2}{2}\|\overline{U}_2^\theta\|\end{bmatrix}\right\}dS=\begin{bmatrix}\alpha_1(1+\nu_1)\\ \alpha_2(1+\nu_2)\end{bmatrix}\int_{S^+}\Lambda\frac{1}{r}\|\theta^e\|dS,\quad(30)$$

where α is the coefficient of linear thermal expansion, and superscript "θ" here means that related physic quantities are induced by thermal loading. Comparing Eq. (29) to Eq. (30), corresponding displacement discontinuities $\|U^\theta\|$ and $\|W^\theta\|$ can be solved by

$$\begin{bmatrix}L_1 & L_{w1}\\ L_2 & L_{w2}\end{bmatrix}\begin{bmatrix}\|U^\theta\|\\ \|W^\theta\|\end{bmatrix}=\frac{\beta}{4\pi L_h}\begin{bmatrix}\dfrac{L_{1\theta}(2-\nu_1)}{2(1+\nu_1)\alpha_1}\|U_1^\theta\|\\[10pt]\dfrac{L_{2\theta}(2-\nu_2)}{2(1+\nu_2)\alpha_2}\|U_2^\theta\|\end{bmatrix},$$

$$\begin{bmatrix}\overline{L}_1 & \overline{L}_{w1}\\ \overline{L}_2 & \overline{L}_{w2}\end{bmatrix}\begin{bmatrix}\|\overline{U}^\theta\|\\ \|\overline{W}^\theta\|\end{bmatrix}=\frac{\beta}{4\pi L_h}\begin{bmatrix}\dfrac{L_{1\theta}\nu_1}{2(1+\nu_1)\alpha_1}\|\overline{U}_1^\theta\|\\[10pt]\dfrac{L_{1\theta}\nu_2}{2(1+\nu_2)\alpha_2}\|\overline{U}_2^\theta\|\end{bmatrix}.$$

$$(31)$$

Note that ν_1 and ν_2 should also satisfy Eq. (23). The corresponding thermal stress intensity factors for 2D hexagonal QCs can be derived by inserting Eq. (26) into Eq. (16) or Eqs. (7b, c) as

$$\begin{bmatrix}K^F\\ K^H\end{bmatrix}^\theta=\frac{\sqrt{2\pi}\,\pi\beta}{4\pi L_h}\lim_{\rho\to0}\left(\begin{bmatrix}\dfrac{L_{1\theta}(2-\nu_1)}{2(1+\nu_1)\alpha_1}\|U_1^\theta\|\\[10pt]\dfrac{L_{2\theta}(2-\nu_2)}{2(1+\nu_2)\alpha_2}\|U_2^\theta\|\end{bmatrix}+\begin{bmatrix}\dfrac{L_{1\theta}\nu_1}{2(1+\nu_1)\alpha_1}\|\overline{U}_1^\theta\|\\[10pt]\dfrac{L_{1\theta}\nu_2}{2(1+\nu_2)\alpha_2}\|\overline{U}_2^\theta\|\end{bmatrix}\right)\frac{1}{\sqrt{\rho}}.\quad(32)$$

Making a comparison between Eqs. (20) and (32), one has

$$\begin{bmatrix} K^{\mathrm{F}} \\ K^{\mathrm{H}} \end{bmatrix}^{\theta} = \frac{2\beta}{L_{\mathrm{h}}} \begin{bmatrix} \dfrac{L_{1\theta}(1-v_1)}{\alpha_1} & 0 \\ 0 & \dfrac{L_{2\theta}(1-v_2)}{\alpha_2} \end{bmatrix} \begin{bmatrix} K_1^e \\ K_2^e \end{bmatrix}, \tag{33}$$

which shows thermal stress intensity factors for 2D hexagonal QCs can also be obtained from corresponding solutions for isotropic thermoelastic materials.

5. Application of ASM to penny-shape crack problems

Suppose the planar crack is a penny-shaped crack centered at the origin of the coordinate system with radius *a*. For an isotropic thermoelastic material, the penny-shaped crack surface is subjected to uniformly distributed combined loadings

$$P(x, y) = p_x + \mathrm{i}p_y = pe^{\mathrm{i}\phi_0}, \quad p_z(x, y) = p_z, \quad h_n(x, y) = -h, \tag{34}$$

where ϕ_0 is defined by $\tan\phi_0 = p_y/p_x$. As the crucial quantities in fracture mechanics, the solutions of EDDs and extended stress intensity factors for the isotropic thermoelastic materials can either be found in many literatures [48-50] or given here directly as follows

$$\left\| u_z^e \right\| = \frac{8(1-v^2)p_z}{E\pi}\sqrt{a^2 - r^2}, \tag{35a}$$

for normal displacement discontinuity, or named crack opening displacement;

$$\left\| U^e \right\| = \frac{16(1-v^2)}{\pi E(2-v)}p\sqrt{a^2 - r^2}\,e^{\mathrm{i}\phi_0}, \tag{35b}$$

for tangential displacement discontinuity induced by tangential loadings;

$$\left\| \theta^e \right\| = \frac{4h}{\beta\pi}\sqrt{a^2 - r^2},$$

$$\left\| U^{\theta} \right\| = \frac{4(1+v)h\alpha}{3\beta\pi}r\sqrt{a^2 - r^2}\,e^{\mathrm{i}\phi}, \tag{35c}$$

for temperature and displacement discontinuities induced by thermal loading, in which $r = \sqrt{x^2 + y^2}$, $\tan\phi = x/y$, extended stress intensity factors are

$$K_I^e = 2\sqrt{\frac{a}{\pi}} p_z, \tag{36a}$$

$$K^e = \frac{2\sqrt{a\pi}}{\pi} p \left(e^{i\Delta\phi} + \frac{v}{2-v} e^{-i\Delta\phi} \right), \tag{36b}$$

$$K_{II}^\theta = \frac{E\alpha h a \sqrt{a}}{3\sqrt{\pi}\beta(1-v)}, \quad K_h = 2\sqrt{\frac{a}{\pi}} h, \tag{36c}$$

where $\Delta\phi = \phi - \phi_0$.

For 2D hexagonal QCs, when crack surfaces are applied with uniformly distributed combined loadings, as

$$p_z(x, y) = p_z, \tag{37a}$$

$$P(x, y) = p_x + i p_y = p e^{i\phi_0},$$
$$Q(x, y) = q_x + i q_y = q e^{i\phi_0}, \tag{37b}$$

$$h_n(x, y) = -h. \tag{37c}$$

We can immediately obtain corresponding crack solutions for 2D hexagonal QCs according to ASM presented in Sections 4,

For Mode I case, using potential function method and complex derivation, Wang et, al. [41] gave an analytical solution for penny-shaped crack. Here, we obtain corresponding crack solutions, e.g. the crack opening displacement by substituting Eq. (35a) into Eq. (10)

$$\|u_z\| = \frac{p_z}{L_3\pi^2} \sqrt{a^2 - r^2}, \tag{38}$$

and get Mode I stress intensity factor by virtue of the substitution of Eq. (36a) into Eq. (11)

18

$$K_{\mathrm{I}}^{\mathrm{F}} = 2\sqrt{\frac{a}{\pi}}\, p_z. \tag{39}$$

Eq. (38) and Eq. (39) are equivalent to Eqs. (40) and (41) in Ref. [40].

Gao and Ricoeur [38] derived an analytical solution of shear field stress intensity factors according to the limited case of spheroidal inclusion. Making use of ASM, the related crack analytical solutions regarding tangential phonon and phason loadings can also be easily established. Combining Eq. (35b) and Eq. (22a), one can obtain tangential EDDs for crucial fracture quantities as,

$$\begin{bmatrix} \|U_1\| \\ \|W_1\| \end{bmatrix} = \frac{\sqrt{a^2 - r^2}}{\pi^2} \begin{bmatrix} L_1 & L_{w1} \\ L_2 & L_{w2} \end{bmatrix}^{-1} \begin{bmatrix} p \\ q \end{bmatrix} e^{i\phi_0}, \tag{40}$$

which show that both phonon and phason loadings influence the tangential EDDs. It is also revealed that phason fields influence on the deformation and fracture of the material. On the other hand, the substitution of Eq. (36b) into Eq. (24) yields

$$\begin{aligned}
K^{\mathrm{F}} &= \frac{2p\sqrt{a\pi}}{\pi}\left(e^{i\Delta\phi} + \frac{v_1}{2 - v_1} e^{-i\Delta\phi} \right), \\
K^{\mathrm{H}} &= \frac{2q\sqrt{a\pi}}{\pi}\left(e^{i\Delta\phi} + \frac{v_2}{2 - v_2} e^{-i\Delta\phi} \right),
\end{aligned} \tag{41}$$

or in a traditional form like

$$\begin{aligned}
K_{\mathrm{II}}^{\mathrm{F}} &= \frac{4\sqrt{a\pi}\, p\cos(\Delta\phi)}{\pi(2 - v_1)}, \\
K_{\mathrm{III}}^{\mathrm{F}} &= \frac{4\sqrt{a\pi}\, p(1 - v_1)\sin(\Delta\phi)}{\pi(2 - v_1)},
\end{aligned} \tag{42a}$$

$$\begin{aligned}
K_{\mathrm{II}}^{\mathrm{H}} &= \frac{4\sqrt{a\pi}\, q\cos(\Delta\phi)}{\pi(2 - v_2)}, \\
K_{\mathrm{III}}^{\mathrm{H}} &= \frac{4\sqrt{a\pi}\, q(1 - v_1)\sin(\Delta\phi)}{\pi(2 - v_2)},
\end{aligned} \tag{42b}$$

where v_1 and v_2 are determined by Eq. (23) and solved as

$$v_1 = \frac{2(\bar{L}_1 L_{w2} - \bar{L}_{w1} L_2)p - 2(\bar{L}_1 L_{w1} - \bar{L}_{w1} L_1)q}{(L_{11} L_{w2} - L_{w11} L_2)p - (L_{11} L_{w1} - L_{w11} L_1)q},$$ (43a)

$$v_2 = \frac{2(\bar{L}_2 L_{w2} - \bar{L}_{w2} L_2)p - 2(\bar{L}_2 L_{w1} - \bar{L}_{w2} L_1)q}{(L_{21} L_{w2} - L_{w21} L_2)p - (L_{21} L_{w1} - L_{w21} L_1)q}.$$ (43b)

From Eqs. (41) and (42), it is found that Mode II and III field intensity factors are very brief in structure, and the phonon and phason loadings are decoupled in Mode II and III field intensity factors. However, when inserting Eq. (43) into (42), we have

$$\begin{bmatrix} K_{\text{II}}^{\text{F}} \\ K_{\text{II}}^{\text{H}} \\ K_{\text{III}}^{\text{F}} \\ K_{\text{III}}^{\text{H}} \end{bmatrix} = \frac{4\sqrt{a\pi}}{\pi} \begin{bmatrix} \kappa_{11} & \kappa_{12} & 0 & 0 \\ \kappa_{21} & \kappa_{22} & 0 & 0 \\ 0 & 0 & \kappa_{33} & \kappa_{34} \\ 0 & 0 & \kappa_{43} & \kappa_{44} \end{bmatrix} \begin{bmatrix} p\cos(\Delta\phi) \\ q\cos(\Delta\phi) \\ p\sin(\Delta\phi) \\ q\sin(\Delta\phi) \end{bmatrix},$$ (44)

where κ_{ij} are the material dependent and are defined by

$$\kappa_{11} = \frac{(L_1 + \bar{L}_1)L_{w2} - (L_{w1} + \bar{L}_{w1})L_2}{2(L_1 L_{w2} - L_{w1} L_2)},$$

$$\kappa_{12} = \frac{L_1 \bar{L}_{w1} - L_{w1} \bar{L}_1}{2(L_1 L_{w2} - L_{w1} L_2)},$$

$$\kappa_{21} = -\frac{L_2 \bar{L}_{w2} - L_{w2} \bar{L}_2}{2(L_1 L_{w2} - L_{w1} L_2)},$$ (45a)

$$\kappa_{22} = -\frac{(L_1 + \bar{L}_1)L_{w1} - (L_{w1} + \bar{L}_{w1})L_1}{2(L_1 L_{w2} - L_{w1} L_2)},$$

$$\kappa_{33} = \frac{(L_1 - \bar{L}_1)L_{w2} - (L_{w1} - \bar{L}_{w1})L_2}{2(L_1 L_{w2} - L_{w1} L_2)},$$

$$\kappa_{34} = -\frac{L_1 \bar{L}_{w1} - L_{w1} \bar{L}_1}{2(L_1 L_{w2} - L_{w1} L_2)},$$

$$\kappa_{43} = \frac{L_2 \bar{L}_{w2} - L_{w2} \bar{L}_2}{2(L_1 L_{w2} - L_{w1} L_2)},$$ (45b)

$$\kappa_{44} = -\frac{(L_1 - \bar{L}_1)L_{w2} - (L_{w1} - \bar{L}_{w1})L_2}{2(L_1 L_{w2} - L_{w1} L_2)}.$$

Observing Eq. (44), we find that the phonon and phason loadings are coupled and they influence field intensity factors simultaneously.

For thermal loading, namely uniform anti-symmetric heat flux applied over the

20

crack surfaces, to our knowledge, no analytical crack solutions for it are found in literature. This is due to the much-complicated coupling effects of the phonon, phason and temperature existing in this problem. It is convenient to be solved by utilizing ASM. Similarly, employing the relationship in Eq. (27) and corresponding solution for thermoelastic materials in Eq. (35c), the temperature discontinuity $\|\theta\|$ induced by thermal loading is obtained as

$$\|\theta\| = -\frac{h}{L_h \pi^2}\sqrt{a^2 - r^2}, \tag{46}$$

and tangential EDDs are solved via the comparison between Eqs. (33) and (35c)

$$\begin{bmatrix} \|U^\theta\| \\ \|W^\theta\| \end{bmatrix} = \frac{h\rho\sqrt{a^2 - r^2}}{3\pi^2 L_h}\begin{bmatrix} L_{11} & L_{w11} \\ L_{21} & L_{w21} \end{bmatrix}^{-1}\begin{bmatrix} L_{1\theta} \\ L_{2\theta} \end{bmatrix}e^{i\phi}, \tag{47}$$

which shows thermal loading can induce both the phonon and phason fields. Because only radial EDDs are incurred by thermal loading which can be indicated in Eq. (47), thermal stress intensity factors must be Mode II cases, which is solved here by inserting Eq. (36c) into Eqs. (28) and (33), as

$$\begin{aligned} \left(K_{II}^F\right)_{ther} &= \frac{2hL_{1\theta}a\sqrt{a}}{3\sqrt{\pi}L_h}, \\ \left(K_{II}^H\right)_{ther} &= \frac{2hL_{2\theta}a\sqrt{a}}{3\sqrt{\pi}L_h}. \end{aligned} \tag{48}$$

Equation (48) indicates that thermal loading induce not only phonon stress intensity factor but also phason stress intensity factor, and both stress intensity factors show difference between $L_{1\theta}$ and $L_{2\theta}$. Moreover, the heat flux intensity factor is solved by

$$K_h = 2\sqrt{\frac{a}{\pi}}h. \tag{49}$$

21

6. Numerical results and discussions

In this section, the results of analytical solutions to the penny-shaped crack are numerically presented to verify the proposed ASM and to assess the influences of phonon-phason coupling effects on fracture parameters of 2D hexagonal QCs. The material constants are chosen as those given in Ref. [38] and listed in Table 1. Making use of these material constants and the definitions in Re. [43] and Appendix B, the material-related constants L_{ij}, L_{wij}, L_3 and L_h in EDD boundary integral equations (5) are calculated and listed as follows,

$$
\begin{aligned}
&L_{11} = 5.559002\,\text{GPa}, \qquad L_{21} = 0.298770\,\text{GPa}, \\
&L_{12} = 3.978748\,\text{GPa}, \qquad L_{22} = 0.218845\,\text{GPa}, \\
&L_{w11} = 0.211817\,\text{GPa}, \qquad L_{w21} = 1.451724\,\text{GPa}, \\
&L_{w12} = 0.547112\,\text{GPa}, \qquad L_{w22} = 3.978748\,\text{GPa},
\end{aligned}
\tag{50a}
$$

$$
\begin{aligned}
&L_{1\theta} = -0.341342\times10^{-4}\,\text{GPa/K}, \\
&L_{2\theta} = 0.176894\times10^{-4}\,\text{GPa/K}, \\
&L_h = -0.421761\,\text{W/(mK)},
\end{aligned}
\tag{50b}
$$

$$
L_3 = 4.814327\,\text{GPa},
\tag{50c}
$$

which are the basic elements to construct the analytical crack solutions by ASM.

6.1. Validity of the present solutions

Using EDD boundary element method, Li et. al. [44] given some useful numerical solutions for rectangular, elliptical and penny-shaped crack problems, in which numerical results about penny-shaped crack with uniform coupled loadings were used to verify the analytical solutions obtained via ASM. Figures 2-7 show the distribution of normalized EDDs across penny-shaped crack surfaces under normal,

tangential, and thermal loadings. Tables 2 tabulates all extended fields intensity factors, which are normalized by

$$F_{\mathrm{I}}^{\mathrm{F}} = \frac{K_{\mathrm{I}}^{\mathrm{F}}\sqrt{\pi}}{2p_z\sqrt{\alpha}}, \tag{51a}$$

$$F_{\mathrm{II}}^{\mathrm{F}} = \frac{K_{\mathrm{II}}^{\mathrm{F}}\sqrt{\pi}}{4\sqrt{a}\,p}, \ F_{\mathrm{III}}^{\mathrm{F}} = \frac{K_{\mathrm{III}}^{\mathrm{F}}\sqrt{\pi}}{4\sqrt{a}\,p},$$

$$F_{\mathrm{II}}^{\mathrm{H}} = \frac{K_{\mathrm{II}}^{\mathrm{H}}\sqrt{\pi}}{4\sqrt{a}\,q}, \ F_{\mathrm{III}}^{\mathrm{H}} = \frac{K_{\mathrm{III}}^{\mathrm{H}}\sqrt{\pi}}{4\sqrt{a}\,q}, \tag{51b}$$

$$\left(F_{\mathrm{II}}^{\mathrm{F}}\right)_{\mathrm{ther}} = \frac{3\sqrt{\pi}L_{\mathrm{h}}\left(K_{\mathrm{II}}^{\mathrm{F}}\right)_{\mathrm{ther}}}{2hL_{1\theta}a\sqrt{a}},$$

$$\left(F_{\mathrm{II}}^{\mathrm{H}}\right)_{\mathrm{ther}} = \frac{3\sqrt{\pi}L_{\mathrm{h}}\left(K_{\mathrm{II}}^{\mathrm{H}}\right)_{\mathrm{ther}}}{2hL_{2\theta}a\sqrt{a}}. \tag{51c}$$

The analytical solutions by ASM are in great agreement with the numerical solutions obtained by EDD boundary element method. To some extent, comparisons of these solutions also validate EDD boundary element method proposed by Li et al. [44].

6.2. Discussion of fracture parameters

As we all known, EDDs and extended stress intensity factors are main fracture parameters and of high significance in fracture analysis. We can see from Figure 3 that phonon displacement discontinuity $\|u_x\|$ along the *x*-axis decreases monotonically with the increase of the applied phason loading. From the point of physic, the phonon displacement represents the deformation of the material. Thus, we can draw a conclusion that the phason loading can alleviate propagation of crack through reducing phonon displacement discontinuity, however, it may promote the quasiperiodic rearrangement of atoms, as predicted form Figure 4. On the other hand,

when applying thermal loadings on the crack surfaces, we can see from Figure 6 and 7 that the generated phonon displacement discontinuities across crack surfaces are opposite to the phason, that is, the influences of thermal effect are difference on the phonon and phason fields.

As regard to extended stress intensity factors, normal phonon stress loading can only induce Mode I phonon stress intensity factor, as discussed in above sections and the literatures [40,43,44,51], which is a simple case and not addressed here. What we are most concerned is the coupled field intensity factors, related to Mode II, III cases, and thermal case, whose corresponding analytical solutions are given firstly in this paper. To quantify the effect of the tangential phonon and phason loadings on the Mode II, III field intensity factors, we convert Eq. (39) to the following form

$$\frac{\sqrt{\pi}}{4\sqrt{a}}\begin{bmatrix} \dfrac{K_{\mathrm{II}}^{\mathrm{F}}}{\kappa_{11}} \\ \dfrac{K_{\mathrm{II}}^{\mathrm{H}}}{\kappa_{22}} \\ \dfrac{K_{\mathrm{III}}^{\mathrm{F}}}{\kappa_{33}} \\ \dfrac{K_{\mathrm{III}}^{\mathrm{H}}}{\kappa_{33}} \end{bmatrix} = \begin{bmatrix} 1 & \varsigma_1 & 0 & 0 \\ \varsigma_2 & 1 & 0 & 0 \\ 0 & 0 & 1 & \varsigma_3 \\ 0 & 0 & \varsigma_4 & 1 \end{bmatrix}\begin{bmatrix} p\cos(\Delta\phi)_x \\ q\cos(\Delta\phi)_x \\ p\sin(\Delta\phi)_y \\ q\sin(\Delta\phi)_y \end{bmatrix}, \tag{52}$$

where $\varsigma_i(i=1,2,3,4)$ are the four ratios of κ_{ij} as

$$\varsigma_1 = \frac{\kappa_{12}}{\kappa_{11}}, \varsigma_2 = \frac{\kappa_{21}}{\kappa_{22}}, \varsigma_3 = \frac{\kappa_{34}}{\kappa_{33}}, \varsigma_4 = \frac{\kappa_{43}}{\kappa_{44}}, \tag{53}$$

and ς_1, ς_2, ς_3, ς_4 characterize the effect of phason loading on $K_{\mathrm{II}}^{\mathrm{F}}$, the effect of phonon loading on $K_{\mathrm{II}}^{\mathrm{H}}$, the effect of phason loading on $K_{\mathrm{III}}^{\mathrm{F}}$, the effect of phonon loading on $K_{\mathrm{III}}^{\mathrm{H}}$, respectively. When the values of ς_i are zero, the phonon and phason stress intensity factors are decoupled and depend directly on the phonon and

phason loadings, respectively. When the values of ς_i are unit, these two stress intensity factors are coupled and influenced by phonon and phason loadings simultaneously. On the other hand, a positive value of ς_i represents these two loadings have a same effect on corresponding stress intensity factor and vice versa. When adopting the material-related constants in Eq. (50), we can obtain

$$\varsigma_1 = -0.0731, \varsigma_2 = 0.0640, \varsigma_3 = 0.1031, \varsigma_4 = -0.0231, \tag{54}$$

which show there are complex effects of the tangential phonon and phason loadings on corresponding field intensity factors for the considered 2D QCs.

Finally, for thermal stress intensity factors, Mode II cases are induced only by thermal loading. Form Eq. (43), the difference between phonon stress intensity factor $\left(K_{\mathrm{II}}^{\mathrm{F}} \right)_{\mathrm{ther}}$ and phason $\left(K_{\mathrm{II}}^{\mathrm{H}} \right)_{\mathrm{ther}}$ are caused by material-related constants $L_{1\theta}$ and $L_{2\theta}$, which have opposite quantities for present constants in Eq. (50). This reveals that thermal loading also has different effect on these two types of thermal stress intensity factors.

7. Conclusion

Considering combined normal, tangential, and thermal loadings for Model I, II, and III crack problems, an analysis solution method, namely ASM, is proposed for 3D planar cracks of arbitrary shape in 2D hexagonal QC media. EDD boundary integral equations governing 3D crack problems are transferred to integral–differential forms by introducing some complex quantities. By comparing these simplified governing

equations, some significant relationships are revealed from the solutions of planar crack problems for 2D hexagonal QC media and those for isotropic thermoelastic media. The solutions to 3D planar crack problems of 2D hexagonal QCs are formulated by means of to the solution approach to the corresponding solutions of isotropic thermoelastic materials.

Applying presented ASM, analytical solutions of a penny-shaped crack under uniformly disturbed combined loadings are obtained. Especially, analytical solutions of Model II, and III problems considering thermal effect are first presented for 2D hexagonal QC. EDD boundary element method proposed by Li et al. [44] is employed to verify the obtained analytical solutions, and great agreement has been reached. Numerical results are obtained to investigate the influences of phonon-phason couple on fracture parameters of 2D hexagonal QCs. Four parameters $\varsigma_i(i=1,2,3,4)$ defined by ratios of κ_{ij} are introduced to quantify the effect of the tangential phonon and phason loadings on corresponding field intensity factors. Additionally, the result indicates that anti-symmetrically thermal loading can only induce Mode II phonon and phason stress intensity factors, and they only have difference on the material-related constants between $L_{1\theta}$ and $L_{2\theta}$.

The present analytical solutions may serve as benchmarks for computational fracture mechanics of 2D hexagonal QCs. The proposed method in this paper provided a way to investigate crack problems of 2D hexagonal QCs through their comparison to corresponding solutions (regardless of analytical or numerical solutions) of isotropic thermoelastic materials.

Acknowledgements

Appendix A: Basic equations for 2D hexagonal QCs [39, 43]

The equilibrium equations in the absence of a body force and body heat source are

$$\frac{\partial \sigma_{xx}}{\partial x} + \frac{\partial \sigma_{xy}}{\partial y} + \frac{\partial \sigma_{zx}}{\partial z} = 0,$$

$$\frac{\partial \sigma_{xy}}{\partial x} + \frac{\partial \sigma_{xy}}{\partial y} + \frac{\partial \sigma_{yz}}{\partial z} = 0, \qquad \text{(A.1a)}$$

$$\frac{\partial \sigma_{zx}}{\partial x} + \frac{\partial \sigma_{yz}}{\partial y} + \frac{\partial \sigma_{xz}}{\partial z} = 0,$$

$$\frac{\partial H_{xx}}{\partial x} + \frac{\partial H_{xy}}{\partial y} + \frac{\partial H_{xz}}{\partial z} = 0,$$

$$\frac{\partial H_{yx}}{\partial x} + \frac{\partial H_{yy}}{\partial y} + \frac{\partial H_{yz}}{\partial z} = 0, \qquad \text{(A.1b)}$$

$$\frac{\partial h_{x}}{\partial x} + \frac{\partial h_{y}}{\partial y} + \frac{\partial h_{z}}{\partial z} = 0. \qquad \text{(A.1c)}$$

The constitutive equations used to describe the relationships of extended stresses and extended displacements are

$$\sigma_{xx} = c_{11}\frac{\partial u_x}{\partial x} + c_{12}\frac{\partial u_y}{\partial y} + c_{13}\frac{\partial u_z}{\partial z} + R_1\frac{\partial w_x}{\partial x} + R_2\frac{\partial w_y}{\partial y} - \lambda_{11}\theta,$$

$$\sigma_{yy} = c_{12}\frac{\partial u_x}{\partial x} + c_{11}\frac{\partial u_y}{\partial y} + c_{13}\frac{\partial u_z}{\partial z} + R_2\frac{\partial w_x}{\partial x} + R_1\frac{\partial w_y}{\partial y} - \lambda_{11}\theta,$$

$$\sigma_{zz} = c_{13}\frac{\partial u_x}{\partial x} + c_{13}\frac{\partial u_y}{\partial y} + c_{33}\frac{\partial u_z}{\partial z} + R_3\frac{\partial w_x}{\partial x} + R_3\frac{\partial w_y}{\partial y} - \lambda_{33}\theta,$$

$$\sigma_{yz} = c_{44}\left(\frac{\partial u_y}{\partial z} + \frac{\partial u_z}{\partial y}\right) + R_4\frac{\partial w_y}{\partial z},$$

(A.2a)

$$\sigma_{zx} = c_{44}\left(\frac{\partial u_x}{\partial z} + \frac{\partial u_z}{\partial x}\right) + R_4\frac{\partial w_x}{\partial z},$$

$$\sigma_{xy} = c_{66}\left(\frac{\partial u_x}{\partial y} + \frac{\partial u_y}{\partial x}\right) + R_6\left(\frac{\partial w_x}{\partial y} + \frac{\partial w_y}{\partial x}\right),$$

$$H_{xx} = R_1\frac{\partial u_x}{\partial x} + R_2\frac{\partial u_y}{\partial y} + R_3\frac{\partial u_z}{\partial z} + K_1\frac{\partial w_x}{\partial x} + K_2\frac{\partial w_y}{\partial y},$$

$$H_{yy} = R_2\frac{\partial u_x}{\partial x} + R_1\frac{\partial u_y}{\partial y} + R_3\frac{\partial u_z}{\partial z} + K_2\frac{\partial w_x}{\partial x} + K_1\frac{\partial w_y}{\partial y},$$

$$H_{xy} = R_6\left(\frac{\partial u_x}{\partial y} + \frac{\partial u_y}{\partial x}\right) + K_3\frac{\partial w_x}{\partial y} + K_6\frac{\partial w_y}{\partial x},$$

$$H_{yx} = R_6\left(\frac{\partial u_x}{\partial y} + \frac{\partial u_y}{\partial x}\right) + K_6\frac{\partial w_x}{\partial y} + K_3\frac{\partial w_y}{\partial x},$$

(A.2b)

$$H_{yz} = R_4\left(\frac{\partial u_y}{\partial z} + \frac{\partial u_z}{\partial y}\right) + K_4\frac{\partial w_y}{\partial z}$$

$$H_{xz} = R_4\left(\frac{\partial u_x}{\partial z} + \frac{\partial u_z}{\partial x}\right) + K_4\frac{\partial w_x}{\partial z}$$

$$h_x = -\beta_{11}\frac{\partial \theta}{\partial x}, \ h_y = -\beta_{11}\frac{\partial \theta}{\partial y}, \ h_z = -\beta_{11}\frac{\partial \theta}{\partial z},$$

(A.2c)

where $c_{ij}(K_i)$ and R_i are the phonon (phason), phonon-phason coupling elastic

constants; λ_{ij} and β_{ij} denote thermal modulus and coefficients of heat conduction,

respectively. The following relations for transversely isotropic hold

$$c_{66} = \frac{c_{11} - c_{12}}{2}, \ K_6 = K_1 - K_2 - K_3, \ R_6 = \frac{R_1 - R_2}{2}.$$

(A.3)

Appendix B: Material related constants [43]

The related material constants in EDDs boundary integral equations are listed as follows

$$
\begin{cases}
L_{11} = \sum_{j=1}^{3} s_{2j}\omega_{1j}A_{2j}^{*}, \\
L_{12} = \sum_{i=1}^{2} s_{1i}f_{1i}A_{1i}^{*}, \\
L_{13} = 3(L_{11} - L_{12}), \\
L_{1\theta} = -\sum_{j=1}^{4} s_{2j}\omega_{1j}D_{j}^{*},
\end{cases}
\qquad
\begin{cases}
L_{w11} = \sum_{j=1}^{3} s_{2j}\omega_{1j}k_{2j}A_{2j}^{*}, \\
L_{w12} = \sum_{i=1}^{2} s_{1i}f_{1i}k_{1i}A_{1i}^{*}, \\
L_{w13} = 3(L_{w11} - L_{w12}),
\end{cases}
\tag{B.1a}
$$

$$
\begin{cases}
L_{21} = \sum_{j=1}^{3} s_{2j}\omega_{1j}B_{2j}^{*}, \\
L_{22} = \sum_{i=1}^{2} s_{1i}f_{1i}B_{1i}^{*}, \\
L_{23} = 3(L_{11} - L_{12}), \\
L_{2\theta} = -\sum_{j=1}^{4} s_{2j}\omega_{1j}D_{j}^{*},
\end{cases}
\qquad
\begin{cases}
L_{w21} = \sum_{j=1}^{3} s_{2j}\omega_{1j}k_{2j}B_{2j}^{*}, \\
L_{w22} = \sum_{i=1}^{2} s_{1i}f_{1i}k_{1i}B_{1i}^{*}, \\
L_{w23} = 3(L_{w21} - L_{w22}),
\end{cases}
\tag{B.1b}
$$

$$
L_{3} = -\sum_{j=1}^{3} \omega_{1j}C_{j}^{*},
\tag{B.1c}
$$

$$
L_{h} = -\frac{s_{24}\beta_{33}}{4\pi},
\tag{B.1d}
$$

where c_{ij}, f_{ij}, β_{ij}, ω_{ij}, $A_{ij}^{*}, B_{ij}^{*}, C_{i}^{*}$, and D_{i}^{*} are the material-related constants defined in Ref. [43], and s_{1i} $(i = 1, 2)$ and s_{2j} $(j = 1, 2, 3)$ with positive real parts are eigenvalues determined by the following eigenvalue equations, respectively,[37]

$$
as_{2}^{6} - bs_{2}^{4} + cs_{2}^{2} - d = 0,
\tag{B.2a}
$$

$$
es_{1}^{4} - fs_{1}^{2} + g = 0,
\tag{B.2b}
$$

where the constants a, b, c, d, e, f and g are defined in the general solution derived by Yang et al. [39]. It should be pointed out that the governing EDD boundary

integral equations are obtained by Zhao et al. [44] via the general solution with distinct eigenvalues.

References

[1] D. Shechtman, I. Blech, D. Gratias, J.W. Cahn, Metallic phase with long-range orientational order and no translational symmetry, Phys. Rev. Lett. 53 (1984) 1951-1953.

[2] D. Levine, P.J. Steinhardt, Quasicrystals: a new class of ordered structures, Phys. Rev. Lett. 53 (1984) 2477-2480.

[3] International Union of Crystallography, Report of the executive committee for 1991, Acta. Cryst. A 48 (1992) 922-946.

[4] L. Bendersky, Quasicrystal with one-dimensional translational symmetry and a tenfold rotation axis, Phys. Rev. Lett. 55 (1985) 1461-1463.

[5] T. Ishimasa, H. Nissen, Y. Fukano, New ordered state between crystalline and amorphous in Ni-Cr particles, Phys. Rev. Lett. 55 (1985) 511-513.

[6] N. Wang, H. Chen, K.H. Kuo, Two-dimensional quasicrystal with eightfold rotational symmetry, Phys. Rev. Lett. 59 (1987) 1010-1013.

[7] L. Bindi, P.J. Steinhardt, N. Yao, P.J. Lu, Natural Quasicrystals, Science 324 (2009) 1306-1309.

[8] L. Bindi, Y. Nan, L. Chaney, S.H. Lincoln, L. A. Christopher, V.D. Vadim, P. E. Michael, K. Alexander, K. Valery, J. M. Glenn, M.S. William, Y. Marina, J.S.

Paul, Natural quasicrystal with decagonal symmetry, Sci. Rep. 5(2015) 9111.

[9] D.V. Talapin, E.V. Shevchenko, M.I. Bodnarchuk, X.C. Ye, J. Chen, C.B. Murray, Quasicrystalline order in self-assembled binary nanoparticle superlattices, Nature, 461 (2009) 964.

[10] G. Ungar, Y.S. Liu, X.B. Zeng, V. Percec, W.D. Cho nanoparticle superlattices Giant Supramolecular Liquid Crystal Lattice, Science, 299 (2003) 1208-1211

[11] T. Dotera, Quasicrystals in Soft Matter, Isr. J. Chem. 51 (2011) 1197-1205.

[12] H.S. Elina, Microstructure, fabrication and properties of quasicrystalline Al-Cu-Fe alloys: a review, J. Alloy. Compd. 363 (2004) 150-174.

[13] J.B. Suck, M. Schreiber, P. Häussler, Quasicrystals: An Introduction to Structure, Physical Properties, and Applications, Springer-Verlag, Heidelberg, 2002.

[14] A.I. Ustinov, S.S. Polischuk, Analysis of the texture of heterogeneous Al–Cu–Fe coatings containing quasicrystalline phase, Scripta. Mater. 47 (2002) 881-886.

[15] X.P. Guo, J.F. Chen, H.L. Yu, H.L. Liao, C. Coddet, A study on the microstructure and tribological behavior of cold-sprayed metal matrix composites reinforced by particulate quasicrystal, Surf. Coat. Tech. 268 (2015) 94-98.

[16] J.M. Dubois, New prospects from potential applications of quasicrystalline materials, Mater. Sci. Eng. A 294 (2000) 4-9.

[17] K. Kamiya1, T. Takeuchi, N. Kabeya, N. Wada, T. Ishimasa, A. Ochiai, K. Deguchi, K. Imura1, N.K. Sato, Discovery of superconductivity in quasicrystal. Nat. Commun. 9 (2018) 154.

[18] T.Y. Fan, Mathematical Theory of Elasticity of Quasicrystals and Its Applications, Springer, Beijing, 2011.

[19] J.E.S. Socolar, T.C. Lubensky, P.J. Steinhardt, Phonons, phasons, and dislocations in quasicrystals, Phys. Rev. B 34 (1986) 3345-3360.

[20] J. Sladek, V. Sladek, S.N. Atluri: Path-independent integral in fracture mechanics of quasicrystals, Eng. Fract. Mech., 140 (2015) 61-71.

[21] L.D. Landau, I.E. Lifshitz, Statistical Physics, Pergamon Press, New York, 1980.

[22] P. Bak, Phenomenological theory of icosahedral incommensurate ('quasiperiodic') order in Mn-Al alloys, Phys. Rev. Lett. 54 (1985) 1517-1519.

[23] P. Bak, Symmetry, stability, and elastic properties of icosahedral incommensurate crystals, Phys. Rev. B 32 (1985) 5764-5772.

[24] D. Levine, T.C. Lubensky, S. Ostlund, S. Ramaswamy, P.J. Steinhardt, J. Toner, Elasticity and dislocations in pentagonal and icosahedral quasicrystals, Phys. Rev. Lett. 54 (1985) 1520-1523.

[25] D.H. Ding, W.G.Yang, C.Z. Hu, R.H. Wang, Generalized elasticity theory of quasicrystals, Phys. Rev. B 48 (1993) 7003-7010.

[26] T.Y. Fan, M. Yiu-Wing, Elasticity theory, fracture mechanics, and some relevant thermal properties of quasi-crystalline materials, Appl. Mech. Rev. 57 (2004) 325-343.

[27] Q.H. Qin, S.W. Yu, An arbitrarily-oriented plane crack terminating at interface between dissimilar piezoelectric materials, Int. J. Solids Struct. 34 (1997) 581-590.

[28] Q.H. Qin, General solutions for thermopiezoelectrics with various holes under thermal loading, Int. J. Solids Struct. 37 (2000) 5561-5578.

[29] V.G. Yakhno, H.Ç.Yaslan, Three dimensional elastodynamics of 2D quasicrystals: The derivation of the time-dependent fundamental solution, Appl. Math. Model. 35 (2011) 3092-3110.

[30] R. Mikulla, J. Stadler, F. Krul, H.R. Trebin, P. Gumbsch, Crack propagation in quasicrystals, Phys. Rev. Lett. 81 (1998) 3163.

[31] Q.H. Qin, Fracture Mechanics of Piezoelectric Materials, Southampton, WIT Press, 2001

[32] W.M. Zhou, T.Y. Fan, Plane elasticity problem of two-dimensional octagonal quasicrystals and crack problem, Chin. Phys. Soc. 10 (2001) 743-747

[33] X.F. Li, T.Y. Fan, Y.F. Sun, A decagonal quasicrystal with a Griffith crack, Phil. Mag. A 79 (1999) 1943-1952.

[34] Y.C. Guo, T.Y. Fan, A Mode-II Griffith crack in decagonal quasicrystal, Appl. Mathe. Mech. 22(2001) 1311-1317.

[35] Y.Z. Peng, T.Y. Fan, Perturbation theory of 2D decagonal quasicrystals, Physica B 311(2002) 326-330.

[36] J. Sladek, V. Sladek, S. Krahulec, Ch. Zhang, M. Wünsche: Crack analysis in decagonal quasicrystals by the MLPG, Int. J. Fract. 181 (2013) 115-126.

[37] Y. Gao, B.-S. Zhao, General solutions of three-dimensional problems for two-dimensional quasicrystals, Appl. Math. Model. 33 (2009) 3382-3391.

[38] Y. Gao, A. Ricoeur, Three-dimensional analysis of a spheroidal inclusion in a

two-dimensional quasicrystal body, Philos. Mag. 92 (2012) 4334-4353.

[39] L. Yang, L.L. Zhang, F. Song, Y. Gao, General Solutions for Three-Dimensional Thermoelasticity of Two-Dimensional Hexagonal Quasicrystals and an Application, J. Therm. Stresses 37 (2014) 363-379.

[40] Y.W. Wang, T.H. Wu, X.Y. Li, G.Z. Kang, Fundamental elastic field in an infinite medium of two-dimensional hexagonal quasicrystal with a planar crack: 3D exact analysis, Int. J. Solids Struct. 66 (2015) 171-183.

[41] X.Y. Li, Y.W. Wang, P.D. Li, G.Z. Kang, R. Müller, Three-dimensional fundamental thermo-elastic field in an infinite space of two-dimensional hexagonal quasi-crystal with a penny-shaped/half-infinite plane crack, Theor. Appl. Fract. Mech. 88 (2017) 18-30.

[42] Y. Li, C.Y. Fan, Q.H. Qin, M.H. Zhao, Closed-form solutions of an elliptical crack subjected to coupled phonon–phason loadings in two-dimensional hexagonal quasicrystal media, Math. Mech. Solids. (2018). https://doi.org/10.1177/1081286518807513

[43] M.H. Zhao, Y. Li, C.Y. Fan, G.T. Xu, Analysis of arbitrarily shaped planar cracks in two-dimensional hexagonal quasicrystals with thermal effects. Part I: theoretical solutions, Appl. Math. Model. 57(2018) 583-602.

[44] Y. Li, M.H. Zhao, C.Y. Fan, G.T. Xu, Analysis of arbitrarily shaped planar cracks in two-dimensional hexagonal quasicrystals with thermal effects. Part II: numerical solutions, Appl. Math. Model. 57(2018) 565-582.

[45] Q.H. Qin, Y.W. Mai BEM for crack-hole problems in thermopiezoelectric

materials, Eng. Frac. Mech. 69 (2002) 577-588.

[46] Q.H. Qin, Green's function and boundary elements of multifield materials, Elsevier, Oxford, 2007.

[47] M.H. Zhao, H.Y. Dang, Y. Li, Fan C.Y., G.T. Xu, Displacement and temperature discontinuity boundary integral equation and boundary element method for cracks in three-dimensional isotropic thermal-elastic media. Int. J. Solids Struct. 81 (2015) 179-181.

[48] Y. Li, H.Y. Dang, G.T. Xu, C.Y. Fan, M.H. Zhao, Extended displacement discontinuity boundary integral equation and boundary element method for cracks in thermo-magneto-electro-elastic media, Smart. Mater. Struct. 25 (2016) 085048.

[49] M.K. Kassir, G.C. Sih, Three-dimensional thermoelastic problems of planes of discontinuities or cracks in solids. Dev. Theor. Appl. Mech. 3(1967) 117-146.

[50] M.K. Kassir, G.C. Sih, Three-dimensional crack problems. Mechanics of Fracture, Vol. 2. Noordhoff Interactional Publishing. 1977

[51] Q.H. Qin, Y.W. Mai, A closed crack tip model for interface crack in thermo-piezoelectric materials, Int. J. Solids Struct. 36 (1999) 2463-2479.

Figure captions list：

Figure 1. Arbitrarily shaped planar crack in the quasiperiodic plane oxy of 2D hexagonal QCs

Figure 2. Phonon displacement discontinuity $\|u_z\|$ for normal loadings in the radial direction of penny-shaped crack

Figure 3. Phonon displacement discontinuity $\|u_x\|$ for different applied tangential loadings in the x-axis direction

Figure 4. Phason displacement discontinuity $\|w_x\|$ for different applied tangential loadings in the x-axis direction

Figure 5. Temperature discontinuity $\|\theta\|$ in the radial direction of penny-shaped crack for thermal loading

Figure 6. Phonon displacement discontinuity $\|u_r\|$ in the radial direction of penny-shaped crack for thermal loading

Figure 7. Phason displacement discontinuity $\|w_r\|$ in the radial direction of penny-shaped crack for thermal loading

Table captions list：

Table 1. Material constants for a particular 2D hexagonal quasicrystal

Table 2. Normalized fields intensity factors for Mode I, II, and III with thermal effect considered at the ends of the x-axis
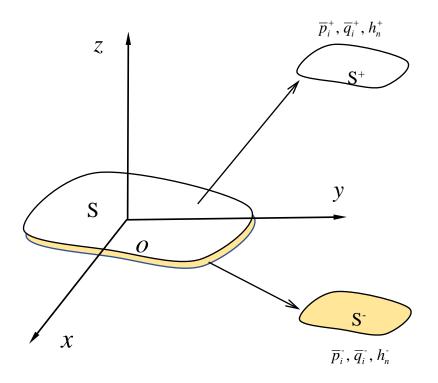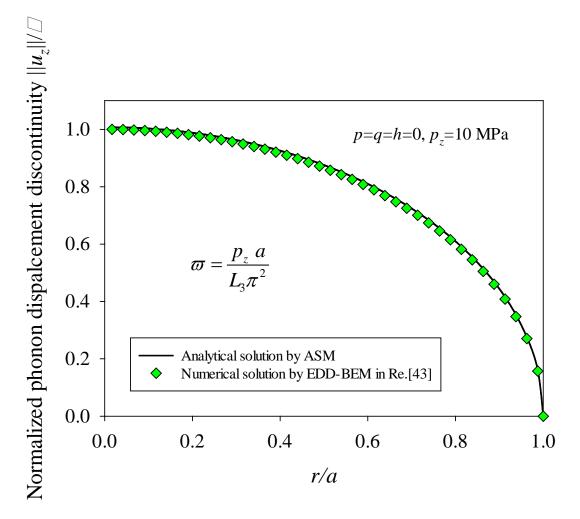
Figure 1. Arbitrarily shaped planar crack in the quasiperiodic plane *oxy* of 2D

hexagonal QCs

Figure 2. Phonon displacement discontinuity $\|u_z\|$ for normal loadings in the radial
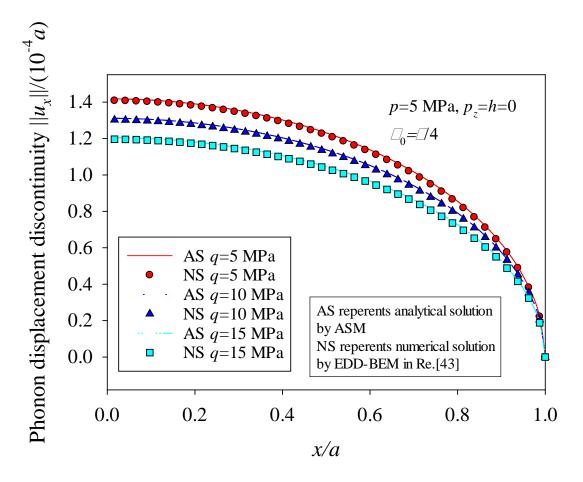
direction of penny-shaped crack

Figure 3. Phonon displacement discontinuity $\|u_x\|$ for different applied tangential
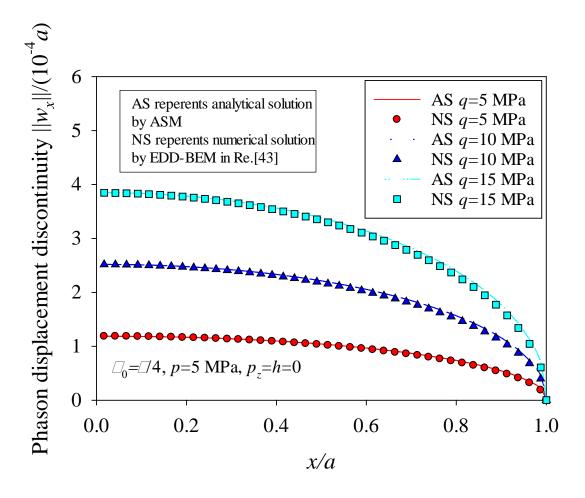
loadings in the *x*-axis direction

Figure 4. Phason displacement discontinuity $\|w_x\|$ for different applied tangential
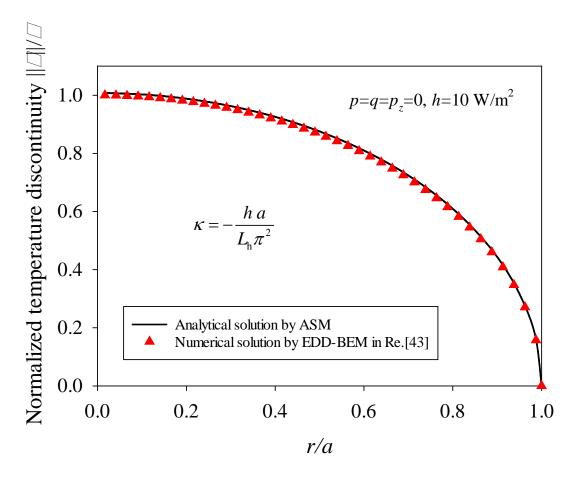
loadings in the x-axis direction

Figure 5. Temperature discontinuity $\|\theta\|$ in the radial direction of penny-shaped
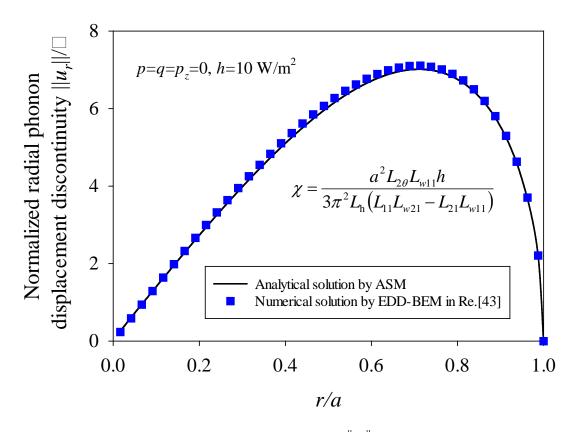
crack for thermal loadings

Figure 6. Phonon displacement discontinuity $\|u_r\|$ in the radial direction of

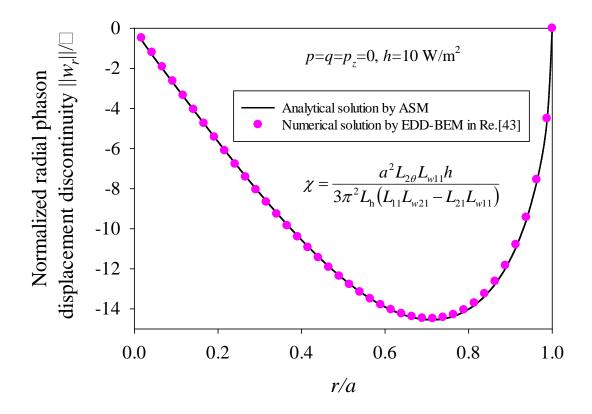penny-shaped crack for thermal loadings

Figure 7. Phason displacement discontinuity $\left\|w_r\right\|$ in the radial direction of

penny-shaped crack for thermal loadings

Table 1. Material constants for a particular 2D hexagonal quasicrystal

Phonon elastic constants	$c_{11} = 200\,\text{GPa}, \quad c_{33} = 150\,\text{GPa}, \quad c_{44} = 50\,\text{GPa}$ $c_{12} = 100\,\text{GPa}, \quad c_{13} = 100\,\text{GPa}$
Phason elastic constants	$K_1 = 50\,\text{GPa}, \quad K_2 = 20\,\text{GPa}$ $K_3 = 20\,\text{GPa}, \quad K_4 = 20\,\text{GPa}$
Phonon-phason coupling constants	$R_1 = 10\,\text{GPa}, \quad R_2 = 5\,\text{GPa}$ $R_3 = 5\,\text{GPa}, \quad R_4 = 5\,\text{GPa}$
Thermal modulus	$\lambda_{11} = 1.798 \times 10^6\,\text{N/(Km}^2), \lambda_{33} = 1.383 \times 10^6\,\text{N/(Km}^2)$
Coefficients of heat conduction	$\beta_{11} = 5.3\,\text{W/(Km)}, \beta_{33} = 5.3\,\text{W/(Km)}$

Table 2. Normalized fields intensity factors for Mode I, II, and III with thermal effect considered at the ends of the *x*-axis

Normalized fields intensity factors	Analytical solutions by ASM	Numerical solutions by EDD-BEM [43]	Relative error (%)
$F_{\mathrm{I}}^{\mathrm{F}}$	1	1.019156	0.018796
$F_{\mathrm{II}}^{\mathrm{F}}$	0.383528	0.386987	0.893828
$F_{\mathrm{III}}^{\mathrm{F}}$	0.323579	0.324310	0.225402
$F_{\mathrm{II}}^{\mathrm{H}}$	0.199334	0.200751	0.680241
$F_{\mathrm{III}}^{\mathrm{H}}$	0.507769	0.509064	0.254388
F^{h}	1	1.017598	1.729366
$\left(F_{\mathrm{II}}^{\mathrm{F}}\right)_{\mathrm{ther}}$	1	0.995833	0.418443
$\left(F_{\mathrm{II}}^{\mathrm{H}}\right)_{\mathrm{ther}}$	1	1.008952	0.887257